Citation Information: 10.1016/j.est.2023.109511

Optimizing the Installation of Hybrid Power Plants in Non-Interconnected Islands

Evangelos E. Pompodakis‡, Georgios C. Kryonidis†, Emmanuel S. Karapidakis‡

‡ Institute of Energy, Environment and Climatic Change, Hellenic Mediterranean University, Greece
† School of Electrical and Computer Engineering, Aristotle University of Thessaloniki, Greece

***Abstract*—This paper proposes a comprehensive optimization approach based on linear programming (LP) for the installation of multiple hybrid power plants (HPPs) in non-interconnected islands. Contrary to the state-of-the-art solutions, the proposed approach optimizes simultaneously the size, location, and technology of each HPP in order to minimize the long-term electricity cost of the island. The optimization problem is formulated as a LP problem to ensure convergence and global optimum solution. Moreover, a series of system constraints are included in the optimization problem, e.g., power reserves, transmission constraints, etc., to ensure the secure and reliable operation of the grid; this is compatible with the actual preventive measures imposed by the network operator in real non-interconnected islands. Simulations are executed in a real Greek Island (Rhodes), confirming the applicability of the proposed method as an optimization tool for network planning studies in non-interconnected islands.**

***Index Terms* — Energy storage systems, hybrid power plant, linear-programming, non-interconnected islands, optimization.**

NOMENCLATURE

Subscripts		
stech	Storage technology, e.g., battery (b), pump (p), compressed air (c), hydrogen (h)	-
g	Thermal generator	-
dsc	Discharge	-
ch	Charge	-
d	direct	-
st	stored	-
b, p, c, h	Battery, PHS, CAES, HSS	
w, s	Wind, Solar	-
Variables		
N_{therm}	Total number of thermal generators	-
N_{hpp}	Total number of HPPs	-
N_{wf}	Total number of existing WFs	-
$cost_g$	Cost of thermal generator g	€/MWh
$\widehat{P^t_{g,therm}}$	Power of thermal generator g at time t	MW
$O\&M_{\iota,dsc,stech}$	O&M cost of discharging block of *stech* of HPP *i*	€/MW
$O\&M_{\iota,ch,stech}$	O&M cost of charging block of *stech* of HPP *i*	€/MW
$O\&M_{\iota,sde,stech}$	O&M cost of storage device of HPP *i*	€/MWh
$O\&M_{\iota,res,w}$	O&M cost of wind generators of HPP *i*	€/MW
$O\&M_{\iota,res,s}$	O&M cost of solar generators of HPP *i*	€/MW
$\widehat{P_{\iota,dsc,stech,inst}}$	Installed (nominal) power of discharging block of *stech* of HPP *i*	MW
$\widehat{P_{\iota,ch,stech,inst}}$	Installed power of charging block of *stech* of HPP *i*	MW
$\widehat{P_{\iota,d,w,inst}}$	Installed power of directly connected wind generators of HPP *i*	MW
$\widehat{P_{\iota,d,s,inst}}$	Installed power of directly connected solar generators of HPP *i*	MW
$\widehat{P_{\iota,st,w,inst}}$	Installed power of wind connected to storage of HPP *i*	MW
$\widehat{P_{\iota,st,s,inst}}$	Installed power of solar connected to storage of HPP *i*	MW
$\widehat{E_{\iota,sde,stech,inst}}$	Installed energy capacity of storage device of *stech* of HPP *i*	MWh
$IC_{\iota,dsc,stech}$	Installation cost of discharging block of *stech* of HPP *i*	€/MW
$IC_{\iota,ch,stech}$	Installation cost of charging block of stech of HPP *i*	€/MW
$IC_{\iota,sde,stech}$	Installation cost of storage device of *stech* of HPP *i*	€/MWh
$IC_{\iota,res,w}$	Installation cost of wind generators of HPP *i*	€/MW
$IC_{\iota,res,s}$	Installation cost of solar generators of HPP *i*	€/MW
$P^t_{k,L}$	Total load of node *k*, at time *t*	MW
$P^t_{\xi,wf}$	Power produced by the existing wind farm ξ at time *t*	MW
$P^t_{\zeta,pv}$	Power produced by the existing photovoltaic plant ζ at time *t*	MW
$\widehat{P^t_{\iota,hpp}}$	Power output of HPP *i* at time *t*	MW
$\widehat{P^t_{\iota,dsc,stech}}$	Discharge power of storage device *stech* of HPP *i* at time *t*	MW
$\widehat{P^t_{\iota,ch,stech}}$	Charge power of storage device *stech* of HPP *i* at time *t*	MW
$\widehat{P^t_{\iota,d,w}}$	Power of directly connected wind generators of HPP *i* at time *t*	MW
$\widehat{P^t_{\iota,st,w}}$	Power of wind generators connected to the storage of HPP *i* at time *t*	MW
$\widehat{P^t_{\iota,d,s}}$	Power of directly connected solar generators of HPP *i* at time *t*	MW
$\widehat{P^t_{\iota,st,s}}$	Power of solar generators connected to the storage of HPP *i* at time *t*	MW
$\varepsilon_{i,dsc,stech}$	Discharging efficiency of *stech of* HPP *i*	-
$\varepsilon_{i,ch,stech}$	Charging efficiency of *stech of* HPP *i*	-
$\widehat{E^t_{\iota,stech}}$	Energy stored in *stech of* HPP *i*	MWh
$\widehat{R^t_{\iota,stech}}$	Reserve power of *stech* of HPP *i*.	MWh
$A_{\iota,land}$	Maximum available land for installing RES within the HPP *i*	MW
$land_{\iota,w}$	Area occupied per MW of installed wind	m^2/MW
$land_{\iota,s}$	Area occupied per MW of installed solar	m^2/MW
$\rho_{i,w}(t)$	Estimated wind power produced per installed MW at the location of HPP *i* at time *t*	-
$\rho_{i,s}(t)$	Estimated solar power produced per installed MW at the location of HPP *i* at time *t*	-
$\widehat{\delta_k}$	Voltage angle of bus *k*	rads
TL_{kl}	Thermal limit of the line between buses *k-l*	
$P_{k,subst}$	Substation power limit of bus k	MW

I. INTRODUCTION

A. Problem Statement and Motivation

Renewable energy sources (RESs) can be used in non-interconnected islands (NIIs) to reduce electricity cost, dependency on the imported fossil fuels, and CO_2 emissions [1],[2]. However, NIIs are usually small or medium size weak networks, where network operators apply a RES penetration limit to ensure frequency stability [3]. Specifically, the instantaneous direct power injection of RESs is restricted up to a percentage of the total load, e.g., 30% in Greece [4] and France [5], curtailing the excess RES power.

To overcome this issue and achieve higher RES penetration levels in NIIs, the solutions proposed in the literature can be

classified into two main categories: a) provision of reserves from RES [6] and b) integration of energy storage systems (ESSs) [1],[2]. Although reserves can untap additional RES penetration in saturated non-interconnected islands, RES curtailment cannot be avoided, especially under high RES generation and low demand periods. The problem can be effectively addressed by introducing ESSs that are connected together with the RESs, thus forming hybrid power plants (HPPs). According to [1],[2], HPPs in non-interconnected islands can enable a total annual RES penetration up to 90%.

B. Literature Review

In the literature, most of the works deal only with the optimal sizing and allocation of ESSs in isolated systems [7]. Specifically, in [8], a differential evolution (DE) algorithm is applied to optimize the size of a hybrid ESS consisting of a battery storage system (BSS) and supercapacitor, so that the frequency violations caused by a wind farm (WF) are eliminated. In [9] and [10], the total network cost is minimized via the optimization of a single storage technology, using mixed-integer linear programming (MILP). In [11], a linear programming (LP) problem is solved to optimize the size of a pumped hydroelectric storage (PHS). However, in all the aforementioned papers, e.g., [8]-[11], the ESSs are optimized as independent entities and not as interconnected and interacting elements within the HPP. Thus, the actual connection and operation of HPPs as well as the interaction between the internal components of HPP is completely ignored in those studies.

Only a few works consider the HPP as a cluster of RESs and ESSs. Specifically, in [12], particle swarm optimization (PSO) and power flow are combined to minimize the total network cost by optimizing the location and size of HPPs. In [13], four representative multi-objective evolutionary algorithms are applied to minimize the levelized cost of energy (LCOE) and the loss of power supply probability (LPSP) by optimizing the size of RESs and a single ESS within the HPP. An improved version of [13] is proposed in [14] by considering hybrid storage (two different storage technologies) within the same HPP. In [15], the total lifecycle cost (TLCC) of an HPP, consisting of RESs and hydrogen storage, is minimized, using heuristic optimization. In [16], a rule-based algorithm is proposed to optimize the battery capacity of an HPP, with the objective to compensate the power variations of RESs. In [17], the authors introduce a rule-based algorithm to minimize the total cost of the Greek island Rhodes, by optimizing the size of a HPP consisting of wind, PHS, and concentrating solar plant. In [2], a rule-based algorithm is proposed to optimize the size of three HPPs for three Greek islands. However, heuristic and rule-based algorithms, e.g., [2],[12]-[17], are characterized by suboptimal solutions, i.e., they cannot ensure the global optimality, and increased computational complexity due to the several iterations needed to converge. Moreover, rule-based algorithms are not applicable in case of multiple HPPs with many internal components, due to the extremely large number of scenarios that need to be computed.

Contrary to heuristic and rule-based algorithms, MILP and LP always find the global optimal as far as it actually exists. In [18] and [19], MILP is applied to optimize the size of a HPP consisting of two RESs and a battery system, while in [20], two complementary ESSs of different technologies are co-optimized to maximize the total HPP revenues. A summary of the state-of-the-art approaches for optimal planning of storage and renewable sources is quoted in Table I at the end of the paper.

None of the existing methods (except [2]) considers into the optimization, the maximum direct renewable's penetration limit that is usually imposed by the network operator to ensure the frequency stability of NIIs. Therefore, in all the aforementioned references, a direct penetration even 100% is allowed, which is not compatible with the preventive measures adopted in several NIIs. Moreover, none of them provides a universal optimization of the sizing, allocation and technology of multiple HPPs in NIIs. Finally, most of them ignore the transmission constraints (thermal limit of substations and lines) as well as the reserve requirements.

C. Aims and Contributions

Scope of the paper is to overcome the limitations of the existing literature, proposing a universal LP optimization approach for NIIs. Its distinct characteristics are below:

- It minimizes the total network cost, through the introduction of HPPs, ensuring the global optimal solution,
- Simultaneous co-optimization of the number, sizing, allocation and technology (e.g., battery, PHS, compressed air, hydrogen, solar, wind etc.) of multiple HPPs,
- The thermal limits of the lines and substations are considered into the optimization as constraints,
- Geographical restrictions of the island are considered, e.g., maximum land area, availability of underground caverns, water reservoirs etc.
- The reserve requirements of HPPs are accounted into the optimization in order to ensure the stability of the network. Reserve provision from HPPs is necessary to cover the reserve deficit caused by the replacement of thermal generators [21].
- The renewable energy sources (RESs) within the HPPs are separated into two groups: RES connected directly to the grid and RES connected to the storage systems. This configuration does not pose any challenge on the frequency stability of the network since storage-connected RESs provide dispatchable power, while grid-connected RESs are imposed a maximum renewable penetration limit according to the preventive rules of each NII.

II. HPP CONFIGURATION

Due to the frequency stability issues of insular networks, the direct RES penetration is curtailed if it exceeds a certain threshold. To reduce the RES curtailments and enable a massive annual renewable penetration, this paper examines the economic feasibility of the total decoupling of a part of RES

units from the grid via their connection to the ESSs, providing dispatchable power.

The internal connection of HPP is shown in Fig. 1. It consists of storage- and grid-connected RESs, the capacity of which is optimized using the proposed optimization formulation, compromising the roundtrip losses of storage-connected RESs and the curtailments of grid-connected RESs. Moreover, it consists of ESSs that enable the simultaneous charge and discharge, using among others, PHS (and/or CAES) with two penstocks and separate turbines and pumps (and/or compressor) [40], [28, Fig. 1], [29, Fig. 1]. Note that supercapacitors, flywheels, and SMESs are only suitable for power quality services with a very low storage capacity, and thus, they are not included in the optimization. The storage-connected RESs are connected to the ESSs via a common HVDC link, eliminating one conversion AC/DC stage for most ESSs and RESs (see Fig.1), increasing the overall efficiency of HPP and reducing its installation cost, compared to whether they were all connected to the grid, as is the case in [21, Fig.1], [28, Fig.1], [20, Fig.1]. The wind turbines are full converter-fed offering a higher annual energy production (AEP), less failures, lower maintenance cost as well as a smaller and lighter size compared to double-fed induction generators (DFIG) [30]. The AC/DC converters enable the pump and compressor to operate with variable speeds, resulting in a higher efficiency, less cavitation issues, as well as the ability to start-up and continuously track renewable power, in contrast to the fixed-speed [31]-[36]. Finally, Proton Exchange Membrane (PEM) electrolyzers have recently been showcasing fast response times [37],[38], thus being able to effectively follow the intermittent RES power producing green hydrogen [39]. It is clarified that the dynamic behavior of HPP of Fig. 1 is out of the scope of this paper and left for future research.

In Fig. 1, $P^{t}_{i,r,j}$ denote the active power of the various components within the HPP *i* at time *t*. Specifically, subscript $r = \{dsc, ch, d, st\}$, where *dsc, ch, d, st* denotes discharged, charged, directly injected, and stored power, respectively. Furthermore, subscript $j = \{b, p, c, h, w, s\}$, where *b, p, c, h, w, s* denote battery, PHS, CAES, HSS, wind and solar power, respectively.

The benefit of this internal connection compared to [21, Fig.1], [28, Fig.1], [20, Fig.1] is that the frequency of the network remains completely unaffected from the variation of $P^{t}_{i,st,w}$ and $P^{t}_{i,st,s}$ since they are decoupled from the network through the storage. Although $P^{t}_{i,d,w}$ and $P^{t}_{i,d,s}$ are directly connected, they never exceed 30% of the load, and thus, their variation does not cause large frequency excursions. Contrarily, in the connections of [20],[21],[28], all RESs are directly connected to the grid, and thus, their intermittent nature may jeopardize the frequency stability of low inertia NII.

In Fig. 1, the direct connection of RESs is favored in case of unsaturated islands with low wind penetration (below 30%) and sufficient margin for accepting, directly, additional renewable power. In the direct RES connection, the renewable power is not subject to round-trip storage losses. However, a portion of this power will may be required to be curtailed in periods of low load demand and high RES production in order to meet the predefined RES penetration limit.

Alternatively, the indirect connection of RES via the ESS is suitable for saturated networks with a high RES penetration (near 30%). This connection mode does not pose any challenge to the frequency stability of the grid since the HPP injects controllable (and uninterrupted) through the discharging blocks of ESSs. To compensate the round-trip losses of ESSs, economic incentives are given to the owners of HPPs, selling the stored energy at higher tariffs than the direct wind energy [22, Table A2], [23, Table I], [24]. Therefore, HPP owner's profit is increased, while the network operator receives indirect benefits due to the mitigation of RES uncertainty by the provision of dispatchable RES power and reserves [23].

III. Proposed Optimization Framework

In this section, the proposed optimization framework is presented for optimizing the installation of multiple HPPs in NIIs. To facilitate the presentation of the mathematical formulation of the optimization problem, the islanded network of Fig. 2 is used as an example, consisting of two thermal generators and existing WFs connected to buses 1 and 4, as well as one existing PV installation connected to bus 3. Moreover, there are three candidate geographical locations for installing HPPs: two of them connected to bus 2 and one to bus 3. The objective of the proposed optimization approach is to find the optimal a) *size*, b) *technology*, and c) *internal connection* of the HPPs, in these three candidate locations that minimize the total energy cost of the network. It is worth mentioning that in case a candidate location is not suitable for installing an HPP, e.g., due to low RES potential, expensive storage cost, transmission/geographical restrictions, etc., the algorithm will yield a zero HPP size for this location, discouraging the HPP installation.

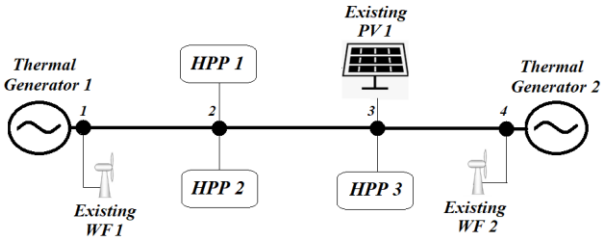

Fig. 2. Example 4-node islanded network with different power generation plants. Loads are may connected to one or more nodes.

A. Objective Function

The total cost of non-interconnected islands is composed by four sub-costs: a) the operation and maintenance (O&M) cost of thermal generators including also fuel cost, b) O&M cost of existing RES units, c) O&M cost of new HPPs, d) installation cost of new HPPs. The first three sub-costs are paid on an annual basis, while the installation cost of new HPPs is paid only once, at the installation stage. To annualize the installation cost of new HPPs, the capital recovery factor (CRF) is used for each component of the new HPPs. As shown in Fig. 1, the HPP consists of the RES units, four charging power blocks (e.g., rectifier, pump, compressor, electrolyzer), four discharging power blocks (e.g., inverter, hydro-turbine, air-turbine, fuel cell), four

storage devices (e.g., battery, water-reservoir, air-reservoir, hydrogen tank). The CRF of each component of HPP is calculated by (1) assuming a given lifecycle (LC) period [19]:

$$CRF_{i,\zeta,j} = \frac{ir\cdot(ir+1)^{LC_{i,\zeta,j}}}{(ir+1)^{LC_{i,\zeta,j}}-1} \quad (1)$$

In (1), *ir* is the interest rate which, in this work, is considered equal to 5%. The subscript i denotes the number of HPP. Subscript ζ={*dsc, ch, sde, res*} where *dsc, ch, sde, res* denote the discharging block, charging block, storage device and RES source, respectively. For instance, $CRF_{1,dsc,p}$ is the CRF of discharging block (*dsc*) of PHS (*p*) of HPP 1.

The cost function of the proposed approach is given in (2) at the end of the paper, assuming an hourly analysis. The symbol $\widehat{\chi}$ denotes that χ is an optimization variable. Equation (2) is composed from the following sub-costs:

1. Cost of thermal generators. This is calculated with respect to the total produced energy[1] throughout the optimization *Horizon* which, in this work, is considered equal to 1 year. N_{therm} is the number of thermal generators, while $cost_g$ and $\widehat{P^t_{g,therm}}$ is the cost and power respectively of thermal generator *g*.
2. Annual O&M cost of renewables and storage. It consists of the O&M costs of the charging power blocks ($O\&M_{i,ch,stech}$), discharging power blocks ($O\&M_{i,dsc,stech}$), storage devices ($O\&M_{i,sde,stech}$) of each technology $stech \in \Phi = \{b, p, c, h\}$, wind ($O\&M_{i,res,w}$) and solar ($O\&M_{i,res,s}$) generators. The O&M of power blocks and renewables is proportional to their installed power (e.g., $P_{i,dsc,\widehat{stech},inst}$), while the O&M of storage device to the energy storage capacity (e.g., $E_{i,sde,\widehat{stech},inst}$).
3. Installation cost (IC) of ESSs and RESs. It consists of the IC of the charging power blocks ($IC_{i,ch,stech}$), discharging power blocks ($IC_{i,dsc,stech}$), storage devices ($IC_{i,sde,stech}$), wind ($IC_{i,res,w}$) and solar ($IC_{i,res,s}$) generators, multiplied by their installed power (e.g., $P_{i,\widehat{d,w},inst}$) or energy (e.g., $E_{i,sde,\widehat{stech},inst}$), all annualized through the CRF.

B. Power Balance Constraints

Eq. (3) ensures the power balance at the output of HPPs. $\widehat{P^t_{i,hpp}}$ is the total power output of HPP *i* at time *t*. All variables are described in Fig. 1 and constrained to be positive in (4).

$$\widehat{P^t_{i,hpp}} = \widehat{P^t_{i,dsc,b}} + \widehat{P^t_{i,dsc,p}} + \widehat{P^t_{i,dsc,c}} + \widehat{P^t_{i,dsc,h}} + \widehat{P^t_{i,d,w}} + \widehat{P^t_{i,d,s}} \quad (3)$$

$$\widehat{P^t_{i,dsc,b}},\ \widehat{P^t_{i,dsc,p}}, \widehat{P^t_{i,dsc,c}}, \widehat{P^t_{i,dsc,h}}, \widehat{P^t_{i,d,w}}, \widehat{P^t_{i,d,s}} \geq 0 \quad (4)$$

$$\forall\ i \in \{1,..,N_{hpp}\} \text{ and } t \in \{1,...,Horizon\}$$

The limit on the direct penetration of RES imposed by the network operator is introduced in (5), where $P^t_{k,L}$ is the load of bus *k* at time *t*, N_{bus} and N_{wf} is the number of buses and existing WFs, respectively, $P^t_{\xi,wf}$ is the power of existing WF ξ at time *t*. Specifically, the total direct RES penetration of all HPPs must be, at any time *t*, lower than a percentage of the total load minus the power of existing WFs. In this paper, this percentage is set equal to 30% [4][5]. In this way, existing WFs are prioritized to share the available RES stability margin.

$$\sum_{i=1}^{N_{hpp}}\left(\widehat{P^t_{i,d,w}} + \widehat{P^t_{i,d,s}}\right) \leq 0.3 \cdot \sum_{k=1}^{N_{bus}}\left(P^t_{k,L}\right) - \sum_{\xi=1}^{N_{wf}}\left(P^t_{\xi,wf}\right) \quad (5)$$

$$\forall\ i \in \{1,..,N_{hpp}\} \text{ and } t \in \{1,...,Horizon\}$$

Inequalities (6) and (7) are introduced to model the possibility of directly connected wind ($\widehat{P^t_{i,d,w}}$) and solar installation ($\widehat{P^t_{i,d,s}}$) to inject power lower than their maximum available power for each HPP and time *t*. Note that $\rho_{i,w}(t)$ and $\rho_{i,s}(t)$ are the normalized estimated powers produced per installed MW of wind and solar generator, respectively, at the location of HPP *i* and time *t*. These values can be available from historical data or measurements throughout the year in that location. In case that the RES limit is exceeded in (5), part of the available direct penetration of RESs in (6)-(7) may be curtailed.

$$\widehat{P^t_{i,d,w}} \leq P_{\widehat{i,d,w},inst} \cdot \rho_{i,w}(t) \quad (6)$$

$$\widehat{P^t_{i,d,s}} \leq P_{\widehat{i,d,s},inst} \cdot \rho_{i,s}(t) \quad (7)$$

$$\forall\ i \in \{1,..,N_{hpp}\} \text{ and } t \in \{1,...,Horizon\}$$

The inequality (8) ensures that the charge power of ESSs is lower than the available power of RES connected to the storage for each HPP *i* and time *t*. Note that all the variables in (8) are shown in Fig. 1. Inequality (8) enables the curtailment of RESs in case ESSs are fully charged. Similar to (6)-(7), inequalities (9) and (10) ensure that the maximum available renewable power is not exceeded for each HPP and time *t*. All variables are constrained to be positive in (11). Finally, it is clarified that the system demand-supply balance equation is not included here since it is indirectly considered in the linear power flow equation system (22). Specifically, adding equations (22a)-(22d) together, the system demand-supply equation is formed.

$$\widehat{P^t_{i,ch,b}} + \widehat{P^t_{i,ch,p}} + \widehat{P^t_{i,ch,c}} + \widehat{P^t_{i,ch,h}} \leq \widehat{P^t_{i,st,w}} + \widehat{P^t_{i,st,s}} \quad (8)$$

$$\widehat{P^t_{i,st,w}} \leq P_{\widehat{i,st,w},inst} \cdot \rho_{i,w}(t) \quad (9)$$

$$\widehat{P^t_{i,st,s}} \leq P_{\widehat{i,st,s},inst} \cdot \rho_{i,s}(t) \quad (10)$$

$$\widehat{P^t_{i,ch,b}}, \widehat{P^t_{i,ch,p}}, \widehat{P^t_{i,ch,c}}, \widehat{P^t_{i,ch,h}}, \widehat{P^t_{i,st,w}}, \widehat{P^t_{i,st,s}} \geq 0 \quad (11)$$

[1] Total cost of thermal generators is the sum of fuel cost and O&M cost. They depend on the generated energy and are given in €/MWh (see Table IV).

C. Storage Constraints

Inequality (12) ensures that the discharge power $\widehat{P^t_{i,dsc,stech}}$ is lower than the maximum limit. $\widehat{R^t_{i,stech}}$ is the required reserve power of *stech* of HPP *i*. Similarly, constraint (13) ensures that the charging power ($\widehat{P^t_{i,ch,stech}}$) is lower than the maximum.

$$\widehat{P^t_{i,dsc,stech}} \leq P_{i\,\widehat{dsc,stech,inst}} - \widehat{R^t_{i,stech}} \quad (12)$$

$$\widehat{P^t_{i,ch,stech}} \leq P_{i,\widehat{ch,stech,inst}} \quad (13)$$

$\forall\, i \in \{1,..,N_{hpp}\}$, $stech \in \{b, p, c, h\}$ and $t \in \{1,...,Horizon\}$

Inequality (14) ensures that the energy stored in *stech* ($e.g., \widehat{E^t_{i,stech}}$) will always lie within the maximum ($\widehat{E_{i,sde,stech,inst}}$) and minimum ($4 \cdot P_{i,\widehat{dsc,stech,inst}}$) capacity limits. Practically, the minimum capacity limit equals to quadruple of nominal discharge power in order to enable HPP to provide 4-hour uninterrupted supply, even under RES outages, ensuring sufficient reserves for a stable supply. $\varepsilon_{i,dsc,stech}, \varepsilon_{i,ch,stech}$ are the discharging and charging efficiencies of *stech*, respectively.

$$4 \cdot P_{i,\widehat{dsc,stech,inst}} \leq \widehat{E^t_{i,stech}} - \frac{\widehat{P^t_{i,dsc,stech}}}{\varepsilon_{i,dsc,stech}} + \widehat{P^t_{i,ch,stech}} \cdot \varepsilon_{i,ch,stech} \leq E_{i,\widehat{sde,stech,inst}} \quad (14)$$

$\forall\, i \in \{1,..,N_{hpp}\}$, $stech \in \{b, p, c, h\}$ and $t \in \{1,...,Horizon\}$

Finally, constraint (15) ensures that the stored energy at the first (0) and last time (*Horizon*) instant are equal.

$$\widehat{E^0_{i,stech}} = \widehat{E^{Horizon}_{i,stech}} \quad \forall\, i \in \{1,..,N_{hpp}\},\ stech \in \Phi = \{b, p, c, h\} \quad (15)$$

D. Geographical Constraints

Constraint (16) ensures that the total area required for the wind and solar installation of each HPP *i* is lower than the maximum available land ($A_{i,land}\ in\ m^2$). $land_{i,w}$ and $land_{i,s}$ (in m^2/MW) is the area occupied per MW of installed wind and solar generators, respectively. In (17)-(18) the capacity of PHS and CAES is restricted by geographical limits ($e.g., E_{i,p,min},\ E_{i,p,max}$). For instance, if there is no an available underground cavern at the location of HPP *i*, for installing a CAES, then $E_{i,c,min} = E_{i,c,max} = 0\ MWh$. Contrarily, no restrictions are imposed on the capacity of battery and HSS.

$$\left(\widehat{P_{i,d,w,inst}} + \widehat{P_{i,st,w,inst}}\right) \cdot land_{i,w} + \left(\widehat{P_{i,d,s,inst}} + \widehat{P_{i,st,s,inst}}\right) \cdot land_{i,s} \leq A_{i,land} \quad (16)$$

$$E_{i,p,min} \leq \widehat{E_{i,sde,p,inst}} \leq E_{i,p,max} \quad (17)$$

$$E_{i,c,min} \leq \widehat{E_{i,sde,c,inst}} \leq E_{i,c,max} \quad (18)$$

E. Reserve Constraints

Power and energy reserves are necessary in insular networks, with high RES penetration, to maintain the frequency stability. Two types of reserves are necessary: a) *short-term (inertial) reserves*, b) *long-term (spinning) reserves*[2]. Inertial reserves are instantaneously provided from the kinetic energy of the rotating masses and restrict the drop of frequency, immediately after the disturbance [6, Fig.2]. Spinning reserves are available by deloading the thermal generators (or HPPs) and using this margin to cover the power deficit, a few seconds after the disturbance [3, Fig. 14].

The minimum inertial reserves are ensured, in the four seasons, through the constraints in (19). Note that $t_{wi}, t_{sp}, t_{su}, t_{au}$ is the sets of hours in winter, spring, summer and autumn, respectively. $N_{min\_wi}, N_{min\_sp}, N_{min\_su}, N_{min\_au}$ is the minimum number of thermal generators to be committed during the four seasons, in order to provide sufficient inertia[3]. The season's discrimination is realized due to the different loads, in the four seasons, especially in touristic islands. In (19), $\widehat{P^{t_{wi}}_{\mu_{wi},therm}}$ expresses the power of thermal generator μ_{wi} at the winter time instant t_{wi}, while $P_{\mu_{wi},therm,min}$ is the technical minima of μ_{wi} thermal generator etc.

Winter: $$\widehat{P^{t_{wi}}_{\mu_{wi},therm}} \geq P_{\mu_{wi},therm,min} \quad (19a)$$
$\forall\, t_{wi} \in \{1,..., \frac{Horizon}{4}\}$, $\mu_{wi} \in \{1,..., N_{min\_wi}\}$

Spring: $$\widehat{P^{t_{sp}}_{\mu_{sp},therm}} \geq P_{\mu_{sp},therm,min} \quad (19b)$$
$\forall\, t_{sp} \in \{\frac{Horizon}{4},..., \frac{2 \cdot Horizon}{4}\}$, $\mu_{sp} \in \{1,..., N_{min\_sp}\}$

Summer: $$\widehat{P^{t_{su}}_{\mu_{su},therm}} \geq P_{\mu_{su},therm,min} \quad (19c)$$
$\forall\, t_{su} \in \{\frac{2 \cdot Horizon}{4},..., \frac{3 \cdot Horizon}{4}\}$, $\mu_{su} \in \{1,..., N_{min\_su}\}$

Autumn: $$\widehat{P^{t_{au}}_{\mu_{au},therm}} \geq P_{\mu_{au},therm,min} \quad (19d)$$
$\forall\, t_{au} \in \{\frac{3 \cdot Horizon}{4},..., Horizon\}$, $\mu_{au} \in \{1,..., N_{min\_au}\}$.

Thermal generators are assigned to provide spinning reserves as well, by loading them up to 90% of their maximum power capacity ($P_{g,therm,max}$ in (20)). For stability reasons, HPPs should also undertake spinning reserves since they replace thermal generators. In (21), the spinning reserves of storage systems must be at least 10% of their installed power. This constraint, combined with (12), ensures that the discharge power blocks have always a 10% available power to contribute to the network frequency control, in a similar sense as thermal generators.

$$0 \leq \widehat{P^t_{g,therm}} \leq 0.9 \cdot P_{g,therm,max} \quad (20)$$

$$\widehat{R^t_{i,stech}} \geq 0.1 \cdot P_{i,\widehat{dsc,stech,inst}} \quad (21)$$
$\forall\, t \in \{1,..., Horizon\}$, $g \in \{1,..,N_{therm}\}$, $i \in \{1,..,N_{hpp}\}$, $stech \in \{b, p, c, h\}$,

[2] Permanent (spinning) reserves include the primary and secondary reserves.

[3] In addition to thermal generators, Hydro- and Air-turbines of HPPs contribute extra inertial reserves included in their rotating masses.

It is clarified that the directly connected RESs are already imposed a RES limit (30% in Greece), and thus, no further deloading for spinning reserves should be required.

F. Transmission Constraints

A linearized power flow model is used here to compute the power flows of the NIIs. Taking as an example the Network of Fig. 2, the power flow of nodes 1-4 is expressed by equations (22a)-(22d), respectively. In (22a), $P_{1,L}^t, P_{1,wf}^t, \widehat{P_{1,therm}^t}$ are the load, WF and thermal generator power of node 1, respectively. $B_{12} = \frac{150kV^2}{X_{12}}$, where $150kV$ is the high voltage (HV) of Rhodes, while X_{12} is the line reactance between nodes 1-2. $\widehat{\delta_1}$ and $\widehat{\delta_2}$ are the voltage angles of nodes 1 and 2. Similarly, for the other nodes, in equations (22b) – (22d).

$$P_{1,L}^t - P_{1,wf}^t - \widehat{P_{1,therm}^t} = B_{12} \cdot \left(\widehat{\delta_2} - \widehat{\delta_1}\right) \quad (22a)$$

$$P_{2,L}^t - \widehat{P_{1,hpp}^t} - \widehat{P_{2,hpp}^t} = B_{21} \cdot \left(\widehat{\delta_1} - \widehat{\delta_2}\right) + B_{23} \cdot \left(\widehat{\delta_3} - \widehat{\delta_2}\right) \quad (22b)$$

$$P_{3,L}^t - P_{1,pv}^t - \widehat{P_{3,hpp}^t} = B_{32} \cdot \left(\widehat{\delta_2} - \widehat{\delta_3}\right) + B_{34} \cdot \left(\widehat{\delta_4} - \widehat{\delta_3}\right) \quad (22c)$$

$$P_{4,L}^t - P_{2,wf}^t - \widehat{P_{2,therm}^t} = B_{34} \cdot \left(\widehat{\delta_3} - \widehat{\delta_4}\right) \quad (22d)$$

In (23), all voltage angles are restricted, while $\widehat{\delta_1}$ is the reference angle equal to zero.

$$\widehat{\delta_1} = 0 \quad \text{and} \quad -\pi \le \widehat{\delta_2}, \widehat{\delta_3}, \widehat{\delta_4} \le \pi \quad (23)$$

Equations (24a)-(24c) restrict the power of each line (e.g., $B_{12} \cdot \left(\widehat{\delta_1} - \widehat{\delta_2}\right)$) to be lower than the thermal limit of the line $(e.g., TL_{12})$.

$$-TL_{12} \le B_{12} \cdot \left(\widehat{\delta_1} - \widehat{\delta_2}\right) \le TL_{12} \quad (24a)$$

$$-TL_{23} \le B_{23} \cdot \left(\widehat{\delta_2} - \widehat{\delta_3}\right) \le TL_{23} \quad (24b)$$

$$-TL_{34} \le B_{34} \cdot \left(\widehat{\delta_3} - \widehat{\delta_4}\right) \le TL_{34} \quad (24c)$$

Finally, equations (25) restrict the total power injected/consumed by the substation of each bus *k*, in order for the maximum substation limit $(P_{k,subst})$ not to be exceeded.

$$P_{1,L}^t - P_{1,wf}^t - \widehat{P_{1,therm}^t} \le P_{1,subst} \quad (25a)$$

$$P_{2,L}^t - \widehat{P_{1,hpp}^t} - \widehat{P_{2,hpp}^t} \le P_{2,subst} \quad (25b)$$

$$P_{3,L}^t - P_{1,pv}^t - \widehat{P_{3,hpp}^t} \le P_{3,subst} \quad (25c)$$

$$P_{4,L}^t - P_{2,wf}^t - \widehat{P_{2,therm}^t} \le P_{4,subst} \quad (25d)$$

G. Relaxation to LP formulation

In the examined problem, HSS and battery capacity are continuous optimization variables ranging from zero up to a (theoretically) infinite value. Therefore, selection (binary) variables are not necessary since in case a component is not selected due to economic infeasibility, its size is automatically set to zero by the LP optimization solver.

Contrarily, CAES and PHS are subject to geographical restrictions between a minimum and maximum capacity (see (17)-(18)). Inevitably, the selection or not of these storage technologies should be represented through selection (binary) variables. However, due to the fact that available locations for installing a CAES or PHS are limited in islands (usually one or two), the selection of these technologies is performed in a form of what-if scenarios. Specifically, after finding an available location for say a CAES, the optimization algorithm is run for two cases: with and without the CAES, namely setting in (18) $E_{i,c,min}, E_{i,c,max} \neq 0$ as well as $E_{i,c,min}, E_{i,c,max} = 0$. In this way, the economic feasibility of CAES is evaluated, while avoiding the binary variables, keeping the LP nature of the optimization.

Traditionally, the unit commitment (UC) of thermal generators is modelled using binary variables for specifying whether a unit is online or not. Thus, the formulated equations include binary or integer variables, forming a MILP problem [26]. However, MILP is still very time-consuming when applied in network with many optimization variables. For instance, planning studies are required to be performed considering long optimization horizons, e.g., 1 year, in order to account for all possible hourly and seasonal correlations between renewable production and demand, making the solution of MILP impossible.

The proposed formulation consists of 665,873 variables 1,538,879 single equations as a result of the long optimization horizon as well as the many components within each HPP. Therefore, the inclusion of binary or integer variables would make the problem unsolvable. Several solutions have been proposed to reduce the computation time of UC of thermal generators such as: a) reducing optimization horizon to say 1 week, missing out on capturing all the seasonal characteristics [26], b) grouping thermal generators with similar characteristics to reduce the number of units [27] and c) LP relaxation where UC is relaxed to a linear formulation [26]. The last approach has been adopted in this paper, as explained in section III.E.

IV. CASE STUDY IN THE ISLAND OF RHODES

A. System Under Study

The HV network of Rhodes is depicted in Fig. 3, consisting of 7 nodes (HV substations). The numbering and capacity of each substation is depicted in Table II. Two thermal power plants and 5 WFs are connected to the network as shown in Fig. 3. The characteristics of WFs and thermal power plants are given in Tables III and IV, respectively. The distance, impedance and thermal limits of the lines, between the substations, are illustrated in Table V. The total load as well as the existing wind and solar power of the island, throughout the year, are depicted in Fig. 4. The total load and solar power are distributed to the substations of Soroni, Ialissos, Rodos, Rodini, Afantou, South Rhodes, Gennadi, in a proportion of 9.8 %, 25.9 %, 14.4 %, 17.3 %, 22.0 %, 3.5 %, 7.0 %, respectively. The total wind is distributed to WFs depending on their installed power, according to Table III.

B. *Cost of Renewables and Storage*

The characteristics of renewables is shown in Table VI. They have a lifetime of 20 years, while wind has a higher power density per occupied land. The costs, lifetime and efficiencies of all common storage technologies are quoted in the supplementary material. They have been taken from the extensive study carried out in [25]. Specifically, the authors in [25] provide indicative breakdown costs for both the storage device and the charging/discharging power blocks. According to [25], the examined storage technologies present completely different characteristics. For instance, lithium-ion batteries have the lowest cost for the charging/discharging power blocks and the highest efficiency, but also, the highest cost and shortest lifetime of storage device. Contrarily, hydrogen has the cheapest storage device but the most expensive power blocks and the lowest efficiency. As a result, each type of storage is suitable for a certain application, e.g., for short-term or long-term storage. Therefore, the economic viability of each type of storage is highly dependent on the needs of the specific network.

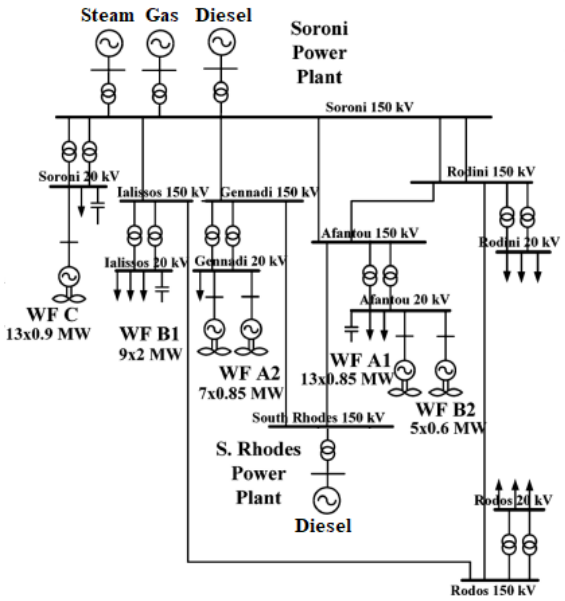

Fig. 3. High-voltage (150 kV) islanded network of Rhodes [3]. The numbering of nodes is quoted in Table II.

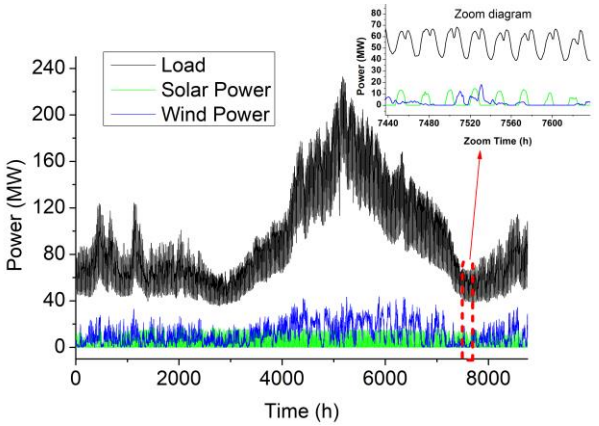

Fig. 4. Total load, wind and solar power, produced in the whole island, throughout the year 2021

TABLE II
Substation Maximum Power

Node (Substation) No.	Substation Name	Maximum Power
1	Soroni*	250 MW
2	Ialissos	66.3 MW
3	Rodos	36.8 MW
4	Rodini	44.2 MW
5	Afantou	56.2 MW
6	South Rhodes*	150 MW
7	Gennadi	17.9 MW

*Soroni and South Rhodes substations are assumed of high power since they connect high-power thermoelectric power plants.

TABLE III
Installed Wind Farms in the Island of Rhodes [3]

Wind Farm	WT type	Maximum Power (MW)
WF A1	DFIG	13x0.85=11.05
WF A2	DFIG	7x0.85=5.95
WF B1	PMSG	9x2=18
WF B2	PMSG	5x0.6=3
WF C	ASIG	13x0.9=11.7

TABLE IV
Characteristics and Cost of Thermal Power Plants in Rhodes

Unit	Nominal Power (MW)	Fuel	Con-sumption (kg or L/MWh)	Fuel cost (€/kg or €/lt)	Carbon Emission* (kg CO_2/MWh)	O&M cost (€/ MWh)
Soroni Power Plant						
Steam Turbine 1	14.5	Mazut	322	0.405 €/kg	266	91
Steam Turbine 2	14.5	Mazut	322	0.405 €/kg	266	91
Gas Turbine 1	17.5	Diesel	525	0.915 €/lt	266	91
Gas Turbine 2	20	Diesel	368	0.915 €/lt	266	91
Gas Turbine 3	18	Diesel	407	0.915 €/lt	266	91
Gas Turbine 4	26.5	Diesel	356	0.915 €/lt	266	91
Diesel Generat. 1	10.5	Mazut	206	0.405 €/kg	266	91
Diesel Generat. 2	10.5	Mazut	206	0.405 €/kg	266	91
Diesel Generat. 3	18	Mazut	225	0.405 €/kg	266	91
Diesel Generat. 4	18	Mazut	225	0.405 €/kg	266	91
Diesel Generat. 5	18	Mazut	225	0.405 €/kg	266	91
South Rhodes Power Plant						
Diesel Generat. 1	17.1	Mazut	205	0.405 €/kg	266	91
Diesel Generat. 2	17.1	Mazut	205	0.405 €/kg	266	91
Diesel Generat. 3	17.1	Mazut	205	0.405 €/kg	266	91
Diesel Generat. 4	17.1	Mazut	205	0.405 €/kg	266	91
Diesel Generat. 5	17.1	Mazut	205	0.405 €/kg	266	91
Diesel Generat. 6	17.1	Mazut	205	0.405 €/kg	266	91
Diesel Generat. 7	17.1	Mazut	205	0.405 €/kg	266	91

*The cost of carbon dioxide credit is considered 0.044 €/kg, according to the 2021 prices.

TABLE V
Characteristics of the Lines

Nodes	Distance (km)	Impedance (Ω/km)	Thermal limit (MW)
1-2	19.6	0.1528 + 0.4492j	140*
1-4	25.2	0.0764 + 0.2246j	280**
2-3	9	0.1528 + 0.4492j	140
3-4	3.9	0.1528 + 0.4492j	140
4-5	18.3	0.1528 + 0.4492j	140
5-6	65	0.1528 + 0.4492j	140
1-5	16.2	0.1528 + 0.4492j	140
6-7	26.4	0.1528 + 0.4492j	140
1-7	53	0.1528 + 0.4492j	140

*Overhead ACSR conductors with maximum current 540A were assumed for all lines, **Two parallel ACSRs

TABLE VI
COST PARAMETERS FOR WIND AND SOLAR INSTALLATIONS [13],[18]

Cost	Wind Installation	Solar Installation
Installation Cost (€/kW)	1850	1220
Yearly O&M Cost (€/kW)	40	20
Life time (years)	20	20
Power density ($land_{i,w}, land_{i,s}$)	10.000 m²/MW	20.000 m²/MW

C. Optimization Results

Battery and hydrogen storage systems can be installed everywhere on the island, without depending on the particular morphology of the island. On the opposite, a PHS requires a favorable geographical location for the reservoir [2],[17], while a CAES prerequisites the availability of a deep underground cavern, e.g., salt dome, depleted natural gas cavern, aquifer, hard rock mines [25]. Specifically, for the island of Rhodes, authors in [17, section 3.3] pointed out a favorable location (most probably the only one), for hosting a seawater PHS, near the substation of Afantou (node 5). On the other hand, we did not find data about favorable locations of CAES, and as a result, we carried out this study, in the form of scenarios. Specifically, the following scenarios were assumed:

- *Base case (current condition)*: It represents the network of Rhodes as it is right now (see section IV.A), without installing any new wind, solar or storage component.
- *Scenario 1*: The network accommodates additional renewable and storage power in the form of HPPs. One candidate HPP per node is examined in the optimization. Only one favorable location for PHS is assumed at node 5, with a maximum reservoir's capacity 5 GWh [17] (namely $E_{5,p,max} = 5GWh$ in (17)). No favorable location exists for CAES, and thus, the maximum capacity in (18) is set to zero, at all nodes. All nodes are assumed to have 1 km² available space for installing renewables (e.g., $A_{i,land} = 1\ km^2\ \forall\ i \in \{1,2,3,4,6,7\}$ in (16)), except node 5 with $A_{5,land} = 2\ km^2$.
- *Scenario 2*: This is the scenario 1 by including also a favorable location for a CAES at node 5, with a size 300 MWh ≤ $E_{5,\widehat{sde,c,inst}} \leq$ 400 MWh (see (18)).
- *Scenario 3*: This is the scenario 1 by considering the 2030 estimate storage prices. The estimated prices were provided by [25, Figure 2], [25, Figure 7], [25, Figure 6], [25, Figure 8], for Lithium-ion battery, PHS, CAES and hydrogen, respectively.

In all scenarios, the proposed method was coded in GAMS, assuming one HPP at each node. An hourly analysis of the whole year (8760 hours) was carried out. The computation time of GAMS was around 0.5 hours. The breakdown cost of the network for the base and examined scenarios is depicted in Table VII at the end of the paper. Note that in Table VII, the annualized cost of the newly installed components is calculated by the summation of the annualized installation cost and the annual O&M cost. As shown in the table, the total annualized network cost for the base and scenario 1, 2 and 3 is 127.45 million € (MM €), 119.54 MM €, 118.66 MM € and 115.4 MM €, respectively. As a result, the optimized connection of HPPs can result in an annualized cost saving, for the island of Rhodes, around 7.9 million € (6% of total cost) in scenario 1. The availability of a favorable CAES location (scenario 2) as well as the cost reduction of ESSs by 2030 (scenario 3) would result in an additional annual cost reduction by 1 million € and 4 million €, respectively. Moreover, due to the strict stability and reserve constraints adopted in the proposed formulation, the stability of the grid is not compromised after the connection of HPPs. The optimal size of each individual component of the newly installed HPPs (e.g., grid- and storage-connected RESs, power and energy capacity of ESSs), at each node, is provided in Figs. 5-13, for the three investigated scenarios.

Based on the Figs. 5-13, the following observations can be made:

✓ Although Rhodes has an already large portion of direct renewable penetration, additional small capacity can be accepted, in all scenarios. For instance, in Fig. 5, the connection of 34.3 MW direct solar and 18.6 MW direct wind is economical feasible. Note that direct solar is higher because its peak generation coincides with the peak load, and thus, it is subject to less curtailments.

✓ The availability of PHS and CAES in node 5 enables the installation of a large capacity of storage-connected renewables in that node, as shown in Fig. 5, 8, 11. Specifically, the installation of RESs in node 5 is restricted only by the land

constraint (16), e.g., $A_{5,land} = 2 \cdot 10^6\ m^2$. Moreover, despite the roundtrip losses, all RESs of node 5 are storage-connected, in all scenarios, for two reasons: first, they are not affected by the 30% limit of direct RES penetration, and thus, they are not subject to curtailments. Second, they leave space to the RES of the other nodes, where a PHS is not available, to be directly connected.

✓ In all examined scenarios, hybrid storage is the economically most feasible solution. Specifically, batteries contribute high power capacity (low energy to power E/P ratio), due to the low cost and high efficiency of their power blocks. Contrarily, pump, CAES and hydrogen contribute high energy capacity (high E/P ratio), utilizing the low cost of their reservoirs. Indicatively, Fig. 14 depicts the charging and discharging power of a 48-h period, for scenario 1, where net load equals the load minus the direct RES penetration. As shown, the charge and discharge power of batteries are constantly very close (their difference is due to the charge and discharge losses), and thus, no high capacity of the expensive battery is required. Practically, a battery capacity of 135.5 MWh is required, only to ensure 4-hour autonomy imposed in constraint (14). On the opposite, pump operates, only when the stored renewable power surpasses the maximum charge power of the battery (e.g., period 7714-7720 h in Fig. 14). In this way, the proposed optimization exploits both the low cost of battery power blocks and the low cost of water reservoir.

✓ In scenario 2, CAES has a higher energy and power capacity than PHS since both its power blocks and storage device are economically more feasible, assuming that a suitable underground cavern exists.

✓ Looking at Fig. 5., although there is available space of 1 km^2 for installing RESs in nodes 1, 2, 3, 4, 6, 7 (e.g., $A_{i,land} = 1\ km^2\ \forall\ i \in \{1,2,3,4,6,7\}$ in (16)), it has not been occupied for two reasons: First, grid-connected RESs are subject to curtailments making their massive connection unprofitable. Second, the unavailability of a PHS or CAES makes the installation of storage-connected RESs unprofitable in those nodes, due to the still high cost of battery and hydrogen.

✓ Although, with the current prices, hydrogen is not competitive (see scenario 1 & 2), the estimated price drop of electrolysis and fuel cell [25, Fig.8], will possibly make it a cost-effective storage solution by 2030 (see scenario 3), but only in low quantities.

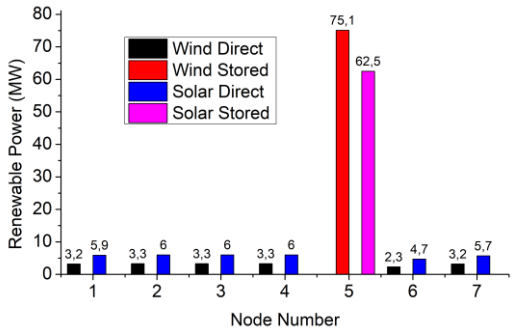

Fig. 5. Optimal installed power of renewables connected directly to the grid and to the storage, at each node of the network, for scenario 1.

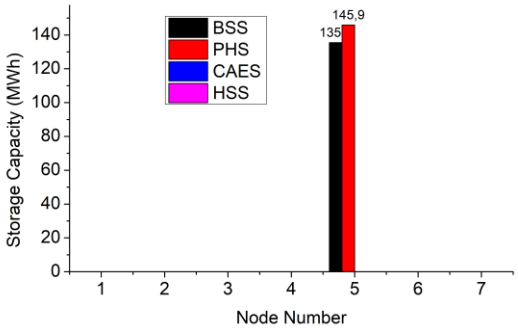

Fig. 6. Optimal installed capacities of the four storage technologies, at each node of the network, for scenario 1.

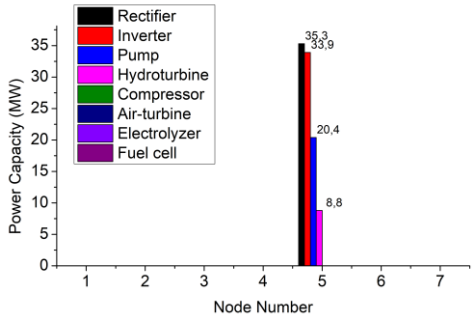

Fig. 7. Optimal installed powers of charging and discharging blocks, at each node of the network, for scenario 1.

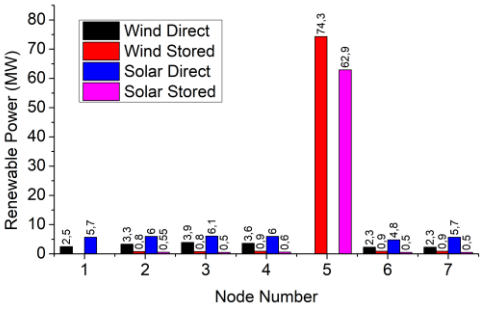

Fig. 8. Optimal installed power of renewables connected directly to the grid and to the storage, at each node of the network, for scenario 2.

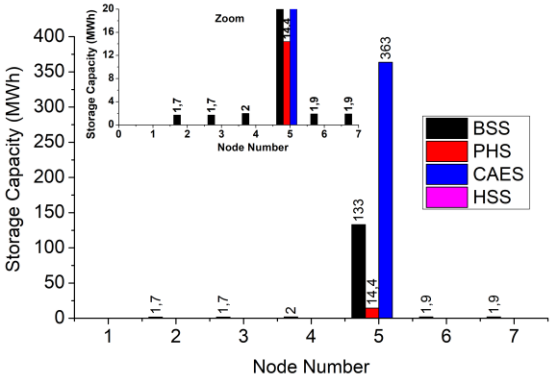

Fig. 9. Optimal installed capacities of the four storage technologies, at each node of the network, for scenario 2.

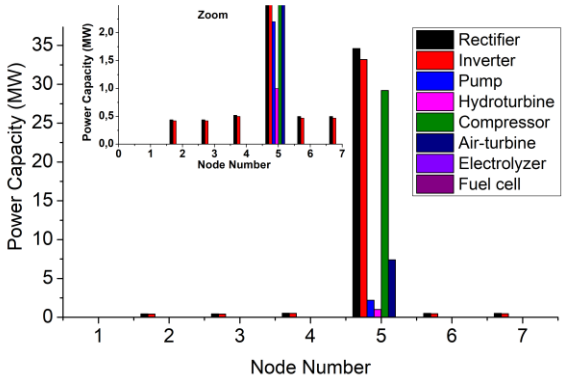

Fig. 10. Optimal installed powers of charging and discharging blocks, at each node of the network, for scenario 2.

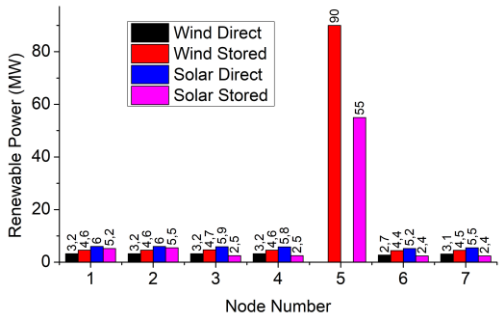

Fig.11. Optimal installed power of renewables connected directly to the grid and to the storage, at each node of the network, for scenario 3.

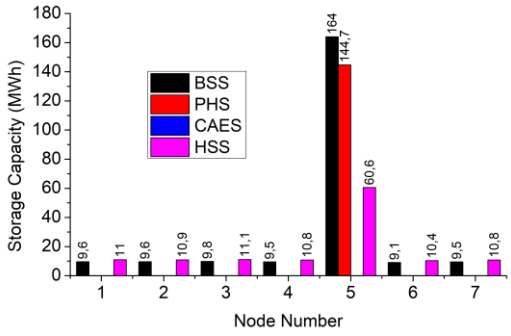

Fig. 12. Optimal installed capacities of the four storage technologies, at each node of the network, for scenario 3.

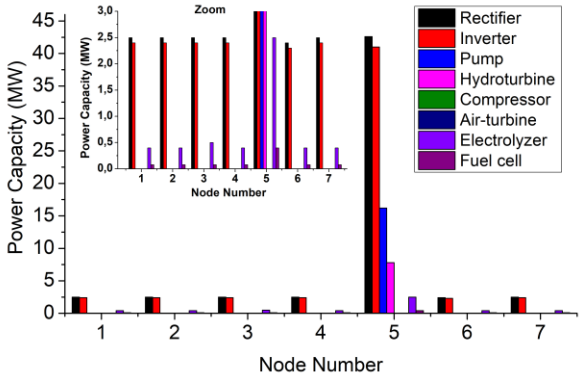

Fig. 13. Optimal installed powers of charging and discharging blocks, at each node of the network, for scenario 3.

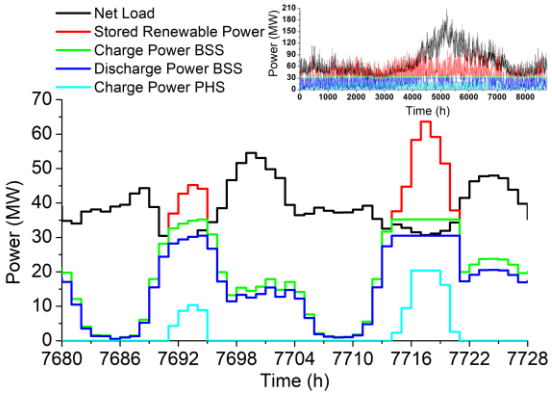

Fig. 14. Charging/discharging sequence of battery and PHS at node 5, for scenario 1.

D. Comparison against existing optimization methods

A comparison of the proposed method against the methods of [19], [12], [2], [17] is presented in Table VII, for scenario 3. References [19] and [12] ignore the RES penetration limit, and thus, a direct RES penetration even 100% is allowed in the mathematical formulation, favoring the direct connection of RESs to the network without using storage as an intermediate layer. However, such an approach is practically inapplicable in real NIIs since they ignore serious restrictions imposed by the network operator of such networks. Therefore, although optimization approaches of [19] and [12] yield a lower annual cost than the proposed method in Table VII, they are unrealistic. The direct RES penetration limit imposed in NIIs is ignored in [13]-[16], [18]-[20] as well, yielding unrealistically optimistic results, in the same sense as [12], [19].

In [2, Fig.6] and [17, Fig.1], the RES penetration limit is considered, complying with the network operator's rules. However, only a single HPP with a single storage technology (e.g., only PHS [17] or BSS [2]) is considered ignoring the complementarity between the storage technologies. Thus, less optimization variables exist in the formulation of [2], [17] and less options for reducing the network's cost. Moreover, they use a rule-based algorithm, without ensuring global optimality of the optimization. Therefore, it yields a sub-optimal solution, as shown in the results of Table VII.

Contrarily to the existing optimization approaches, the proposed optimization formulation considers all the necessary restrictions imposed by the network operators in NIIs, for ensuring the network's stability, deriving a realistic solution. Moreover, in contrast to [2],[12]-[17], the proposed LP formulation ensures that the derived solution presents global optimality.

V. CONCLUSIONS

This paper proposes a generalized linear programming (LP) optimization approach for optimizing the individual components of hybrid power plants (HPPs) in non-interconnected islands. Contrarily to the existing literature, the proposed optimization approach co-optimizes, simultaneously, the size, allocation and technology of multiple HPPs, by considering, accurately, the reserve's requirements, transmission constraints, and maximum renewable's penetration limits usually imposed in insular networks. The renewable energy sources (RESs) within the HPPs are separated into two groups: RES connected directly to the grid and to the storage systems. This configuration does not jeopardize the frequency stability since storage-connected RESs provide dispatchable power, while grid-connected RESs are imposed a maximum renewable penetration limit, which is completely manageable without additional measures. The capacity of RESs is optimized by compromising the roundtrip losses of storage-connected RES with the curtailments of grid-connected RESs. A case study is conducted in the island of Rhode, Greece, to highlight the performance of the proposed optimization method and investigate the economic feasibility of HPPs in a real insular network. Results indicated that the optimal installation of HPPs can result in a reduction of the annual network cost higher than 7.9 million €, corresponding to more than 6% of the annual cost of Rhode.

APPENDIX

A supplementary file including the storage data as well as the optimization code have been submitted along with the manuscript.

REFERENCES

[1] D. Katsaprakakis, "Hybrid power plants in non-interconnected insular systems," *Appl. Energy*, vol. 164, pp. 268-283, 2016.

[2] D. Katsaprakakis, I. Dakanali, and C. Condaxakis, D. Christakis, "Comparing electricity storage technologies for small insular grids," *Appl. Energy*, vol. 251, pp. 84-89, 2019.

[3] I. D. Margaris, S. A. Papathanassiou, N. D. Hatziargyriou, A. D. Hansen and P. Sorensen, "Frequency control in autonomous power systems with high wind power penetration," *IEEE Trans. Sustain. Energy*, vol. 3, no. 2, pp. 189-199, Apr. 2012.

[4] E. E. Pompodakis, G. C. Kryonidis, and E. S. Karapidakis, "Volt/Var control and energy management in non-interconnected insular networks with multiple hybrid power plants," *Appl. Energy*, vol. 331, 2023.

[5] J. I. Sarasúaa, G. M. Lucas, and M. Lafoz, "Analysis of alternative frequency control schemes for increasing renewable energy penetration in El Hierro Island power system," *Int. J. Elect. Power & Energy Sys.*, vol. 113, pp. 807-823, 2019.

[6] Yi Cheng, R. Azizipanah-Abarghooee, S. Azizi, L. Ding, and V. Terzija, "Smart frequency control in low inertia energy systems based on frequency response techniques: A review", *Appl. Energy*, vol. 279, 2020.

[7] L. A. Wong, V. K. Ramachandaramurthy, P. Taylor, J.B. Ekanayake, S. L. Walker, and S. Padmanaban, "Review on the optimal placement, sizing and control of an energy storage system in the distribution network," *J. Energy Storage*, vol. 21, pp. 489-504, 2019.

[8] J. Cao, W. Du, H. Wang, and M. McCulloch, "Optimal sizing and control strategies for hybrid storage system as limited by grid frequency deviations," *IEEE Trans. Power Syst.*, vol. 33, no. 5, pp. 5486-5495, Sept. 2018.

[9] H. Pandžić, Y. Wang, T. Qiu, Y. Dvorkin, and D. S. Kirschen, "Near-optimal method for siting and sizing of distributed storage in a transmission network," *IEEE Trans. Power Syst.*, vol. 30, no. 5, pp. 2288-2300, Sept. 2015.

[10] G. N. Psarros, E. G. Karamanou, and S. A. Papathanassiou, "Feasibility analysis of centralized storage facilities in isolated grids," IEEE Trans. Sustain. Energy, vol. 9, no. 4, pp. 1822-1832, Oct. 2018.

[11] P. D. Brown, J. A. PeÇas Lopes, and M. A. Matos, 'Optimization of pumped storage capacity in an isolated power system with large renewable penetration," *IEEE Trans. Power Syst.*, vol. 23, no. 2, pp. 523-531, May 2008.

[12] C. D. Rodríguez-Gallegos *et al.*, "A siting and sizing optimization approach for PV–battery–diesel hybrid systems," *IEEE Trans. Ind. Appl.*, vol. 54, no. 3, pp. 2637-2645, May-June 2018.

[13] Y. He, S. Guo, J. Zhou, F. Wu, J. Huang, and H. Pei, "The quantitative techno-economic comparisons and multi-objective capacity optimization of wind-photovoltaic hybrid power system considering different energy storage technologies," *Energy Conv. Manag.*, vol. 229, 2021.

[14] Y. He, S. Guo, J. Zhou, J. Ye, J. Huang, K. Zheng, and X. Du, "Multi-objective planning-operation co-optimization of renewable energy system with hybrid energy storages," *Renew. Energy*, vol. 184, pp. 776-790, 2022.

[15] W. Zhang, A. Maleki, M. A. Rosen, J. Liu, "Sizing a stand-alone solar-wind-hydrogen energy system using weather forecasting and a hybrid search optimization algorithm", *Energy Conv. Manag.*, vol. 180, pp. 609-621, 2019.

[16] Y. Yang, S. Bremner, C. Menictas, and M. Kay, "Impact of forecasting error characteristics on battery sizing in hybrid power systems," *J. Energy Storage*, vol. 39, 2021.

[17] G. E. Arnaoutakis, G. Kefala, E. Dakanali, and D. A. Katsaprakakis. "Combined operation of wind-pumped hydro storage plant with a concentrating solar power plant for insular systems: A Case study for the island of Rhodes", *Energies*, vol. 15, no. 18, 2022.

[18] J. C. Alberizzi, J. M. Frigola, M. Rossi, and M. Renzi, "Optimal sizing of a hybrid renewable energy system: Importance of data selection with highly variable renewable energy sources," *Energy Conv. Manag.*, vol. 223, 2020.

[19] A. Malheiro, P. M. Castro, R. M. Lima, and A. Estanqueiro, "Integrated sizing and scheduling of wind/PV/diesel/battery isolated systems," *Renew. Energy*, vol. 83, pp. 646-657, 2015.

[20] M. Khosravi, S. Afsharnia, and S. Farhangi, "Optimal sizing and technology selection of hybrid energy storage system with novel dispatching power for wind power integration," *Int. J. Elect. Power Energy Syst.*, vol. 127, 2021.

[21] S. Papaefthymiou, E. Karamanou, S. Papathanassiou, and M. Papadopoulos, "Operating policies for wind-pumped storage hybrid power stations in island grids," *IET Renew. Power Gener.*, vol. 3, no 3, pp. 293-307, 2009.

[22] S. V. Papaefthymiou and S. A. Papathanassiou, "Optimum sizing of wind-pumped-storage hybrid power stations in island systems," *Renew. Energy*, Vol. 64, pp 187-196, 2014.

[23] A. V. Ntomaris and A. G. Bakirtzis, "Stochastic scheduling of hybrid power stations in insular power systems with high wind penetration," *IEEE Trans. Power Syst.*, vol. 31, pp. 3424-3436, 2016.

[24] Greek Law 4414/2016, https://www.e-nomothesia.gr/energeia/nomos-4414-2016.html.

[25] Mongird, Kendall *et al.* "2020 grid energy storage technology cost and performance assessment," *Tech. Report*, US DOE, 2020.

[26] L. Zhang, T. Capuder and P. Mancarella, "Unified Unit Commitment Formulation and Fast Multi-Service LP Model for Flexibility Evaluation

in Sustainable Power Systems," in IEEE Transactions on Sustainable Energy, vol. 7, no. 2, pp. 658-671, 2016.
[27] B. S. Palmintier and M. D. Webster, "Heterogeneous unit clustering for efficient operational flexibility modeling", IEEE Trans. Power Syst., vol. 29, no. 3, pp. 1089-1098, May 2014.
[28] A. G. Papakonstantinou, A. I. Konstanteas and S. A. Papathanassiou, "Solutions to Enhance Frequency Regulation in an Island System With Pumped-Hydro Storage Under 100% Renewable Energy Penetration," in IEEE Access, vol. 11, pp. 76675-76690, 2023.
[29] Mahdieh Adib, Fuzhan Nasiri, Fariborz Haghighat, Karthik Panchabikesan, Gayathri Venkataramani, Saligram Tiwari, Velraj Ramalingam, "Integrating compressed air energy storage with wind energy system – A review", e-Prime - Advances in Electrical Engineering, Electronics and Energy, Volume 5, 100194, 2023.
[30] Report, "PMG vs. DFIG – the big generator technology debate", The Switch, https://theswitch.com/2014/03/20/pmg-vs-dfig-the-big-generator-technology-debate/
[31] M. Valavi, E. Devillers, J. L. Besnerais, A. Nysveen and R. Nilsen, "Influence of Converter Topology and Carrier Frequency on Airgap Field Harmonics, Magnetic Forces, and Vibrations in Converter-Fed Hydropower Generator," in IEEE Transactions on Industry Applications, vol. 54, no. 3, pp. 2202-2214, 2018.
[32] Yang, X., Yang, C., Yue, C., Yao, D., & Yuan, C., "Optimized Operation of Hydropower Plant with VSC HVDC Unit Connection", CIGRE AORC Technical Meeting, Tokyo, 2014.
[33] P. K. Steimer, O. Senturk, S. Aubert and S. Linder, "Converter-fed synchronous machine for pumped hydro storage plants," 2014 IEEE Energy Conversion Congress and Exposition (ECCE), Pittsburgh, PA, USA, pp. 4561-4567, 2014.
[34] M. Valavi and A. Nysveen, "Variable-Speed Operation of Hydropower Plants: A Look at the Past, Present, and Future," in IEEE Industry Applications Magazine, vol. 24, no. 5, pp. 18-27, Sept.-Oct. 2018.
[35] M. Martínez, M. G. Molina and P. E. Mercado, "Dynamic performance of compressed air energy storage (CAES) plant for applications in power systems," 2010 IEEE/PES Transmission and Distribution Conference and Exposition: Latin America (T&D-LA), Sao Paulo, Brazil, pp. 496-503, 2010.
[36] O. Maisonnave, L. Moreau, R. Aubrée, M.F. Benkhoris, T. Neu, D. Guyomarc'h, "Optimal energy management of an underwater compressed air energy storage station using pumping systems", Energy Conversion and Management, Volume 165, Pages 771-782, 2018.
[37] D. Zarras, A. Papakonstantinou, S. Papathanassiou, "Control of Hydrogen Storage Systems for Primary Frequency Response and Inertia Emulation", IEEE International Conference on Environment and Electrical Engineering and IEEE Industrial and Commercial Power Systems Europe (EEEIC / I&CPS Europe), Madrid, 2023.
[38] Y. Dong, S. Ma, Z. Han, J. Bai, Q. Wang, "Research on the adaptability of proton exchange membrane electrolysis in green hydrogen–electric coupling system under multi-operating conditions", Energy Reports, Volume 9, Pages 4789-4798, 2023.
[39] Val Stori, "Offshore Wind to Green Hydrogen: Insights from Europe", Report of Clean Energy States Alliance, 2021.
[40] D. Al. Katsaprakakis, D. G. Christakis, K. Pavlopoylos, S. Stamataki, I. Dimitrelou, I. Stefanakis, P. Spanos, "Introduction of a wind powered pumped storage system in the isolated insular power system of Karpathos–Kasos", Applied Energy, Volume 97, Pages 38-48, 2012.

$$Cost = \sum_{t=1}^{Horizon} \left(\sum_{g=1}^{N_{therm}} \left(cost_g \cdot \widehat{P^t_{g,therm}} \right) \right)$$
$$+ \sum_{\iota=1}^{N_{hpp}} \left(\sum_{stech \in \Phi} \left(O\&M_{\iota,dsc,stech} \cdot \widehat{P_{\iota,dsc,stech,\iota nst}} + O\&M_{\iota,ch,stech} \cdot \widehat{P_{\iota,ch,stech,\iota nst}} + O\&M_{\iota,sde,stech} \cdot \widehat{E_{\iota,sde,stech,\iota nst}} \right) + O\&M_{\iota,res,w} \cdot \left(\widehat{P_{\iota,d,w,\iota nst}} + \widehat{P_{\iota,st,w,\iota nst}} \right) \right.$$
$$\left. + O\&M_{\iota,res,s} \cdot \left(\widehat{P_{\iota,d,s,\iota nst}} + \widehat{P_{\iota,st,s,\iota nst}} \right) \right)$$
$$+ \sum_{\iota=1}^{N_{hpp}} \left(\sum_{stech \in \Phi} \left(IC_{\iota,dsc,stech} \cdot \widehat{P_{\iota,dsc,stech,\iota nst}} \cdot CRF_{\iota,dsc,stech} + IC_{\iota,ch,stech} \cdot \widehat{P_{\iota,ch,stech,\iota nst}} \cdot CRF_{\iota,ch,stech} + IC_{\iota,sde,stech} \cdot \widehat{E_{\iota,sde,stech,\iota nst}} \cdot CRF_{\iota,sde,stech} \right) + IC_{\iota,res,w} \right.$$
$$\left. \cdot \left(\widehat{P_{\iota,d,w,\iota nst}} + \widehat{P_{\iota,st,w,\iota nst}} \right) \cdot CRF_{\iota,res,w} + IC_{\iota,res,s} \cdot \left(\widehat{P_{\iota,d,s,\iota nst}} + \widehat{P_{\iota,st,s,\iota nst}} \right) \cdot CRF_{\iota,res,s} \right) \quad (2)$$

TABLE I
STATE-OF-THE-ART SOLUTIONS FOR OPTIMAL PLANNING OF STORAGE AND RENEWABLE SOURCES

	Network Type	Multiple HPPs	HPP sizing	HPP technology optimization	HPP detailed modelling	Network Constraints	SR/DRPL* consideration	Optimization Method	Objective function	Optimization Period	Year of publication
Optimization of ESSs and RESs as separate entities											
[8]	GC*	–	ESS	ESS	–	–	DRPL	DE	ESS cost	Several minutes	2018
[9]	GC	–	ESS	–	–	✓	–	MILP	Network cost	1 yr	2015
[10]	ISL	–	ESS	–	–	–	✓	MILP	Network cost	1 yr	2018
[11]	ISL*	–	ESS	–	–	–	✓	LP	Network cost	24 h	2008
Optimization of ESSs and RESs as entities of the HPP											
[12]	ISL	✓	RES/ ESS	–	–	✓	SR	PSO	Network cost	12 days	2018
[13]	ISL	–	RES/ESS	RES	–	–	–	Heuristic	LCOE & LPSP	1 yr	2021
[14]	ISL	–	RES/ESS	RES/ESS	–	–	–	Heuristic	LCOE & LPSP	1 yr	2022
[15]	ISL	–	RES/ESS	–	–	–	–	Heuristic	TLCC	1 month	2019
[16]	GC	-	ESS	-	–	–	–	Rule-based	RES Forecast error	1 yr	2021

[17]	ISL	-	RES	RES	✓	–	✓	Rule-based	Network cost	1 yr	2022
[2]	ISL	-	RES	RES	✓	–	✓	Rule-based	Network cost	1 yr	2019
[18]	ISL	-	RES/ESS	-	–	–	–	MILP	Network cost	1 month	2020
[19]	ISL	-	RES/ESS	RES	–	–	–	MILP	LCOE	1 yr	2015
[20]	GC	-	RES/ESS	ESS	–	–	–	MILP	HPP revenues	1 yr	2021
Proposed	ISL	✓	RES/ESS	RES/ESS	✓	✓	✓	LP	Network cost	1 yr	2023

*GC: Grid-Connected, ISL: Islanded, SR: Spinning Reserves, DRPL: Direct RES penetration limit,

TABLE VII

ANNUAL BREAKDOWN COST OF THE NETWORK FOR THE EXAMINED SCENARIOS*

	Base Case -Proposed	Scenario 1 -Proposed	Scenario 2 -Proposed	Scenario 3 -Proposed	Scenario 3 -Ref. [19]	Scenario 3 -Ref. [12]	Scenario 3-Ref. [2],[17]
Total annual thermal power (GWh)	670.7	388.9	382.4	309.2	349.5	426.2	477.6
Total annual cost of thermal power (MM €)**	**125**	**72.3**	**71.08**	**57.5**	**65**	**79.3**	**88.8**
Total power of existing wind (MW)	49.7	49.7	49.7	49.7	49.7	49.7	49.7
Total annual O&M cost of existing wind (MM €)	**2.09**	**2.09**	**2.09**	**2.09**	**2.09**	**2.09**	**2.09**
Total power of existing solar (MW)	18.2	18.2	18.2	18.2	18.2	18.2	18.2
Total annual O&M cost of existing solar (MM €)	**0.36**	**0.36**	**0.36**	**0.36**	**0.36**	**0.36**	**0.36**
Total power of new wind (MW)	-	93.7	97.2	136	137.3	-	55.5
Annualized cost of new wind (MM €)	**-**	**17.81**	**18.47**	**25.8**	**26.1**	**-**	**10.5**
Total power of new solar (MW)	-	96.8	99.9	104	31.4	182.6	72.2
Annualized cost of new solar (MM €)	**-**	**11.4**	**11.77**	**12.3**	**3.7**	**21.5**	**8.5**
Total capacity of batteries (MWh)	-	135.5	142.3	221.2	-	-	-
Annualized cost of batteries (MM €)	**-**	**10.14**	**10.65**	**11.6**	**-**	**-**	**-**
Total capacity of rectifiers (MW)	-	35.2	37	57.5	-	-	-
Annualized cost of rectifiers (MM €)	**-**	**0.5**	**0.52**	**0.7**	**-**	**-**	**-**
Total capacity of inverters (MW)	-	33.8	35.6	55.3	-	-	-
Annualized cost of inverters (MM €)	**-**	**0.48**	**0.5**	**0.7**	**-**	**-**	**-**
Total capacity of water reservoirs (MWh)	-	145.9	14.4	144.7	-	-	181.8
Annualized cost of water reservoirs (MM €)	**-**	**0.68**	**0.07**	**0.68**	**-**	**-**	**0.8**
Total capacity of pumps (MW)	-	20.4	2.2	16.2	-	-	37.5
Annualized cost of pumps (MM €)	**-**	**2.64**	**0.28**	**2.1**	**-**	**-**	**4.8**
Total capacity of hydroturbines (MW)	-	8.8	1	7.7	-	-	21.1
Annualized cost of hydroturbines (MM €)	**-**	**1.14**	**0.13**	**1.0**	**-**	**-**	**2.7**
Total capacity of air reservoirs (MWh)	-	-	363.7	-	-	-	
Annualized cost of air reservoirs (MM €)	**-**	**-**	**0.14**	-	-	-	
Total capacity of compressors (MW)	-	-	29.2	-	-	-	
Annualized cost of compressors (MM €)	**-**	**-**	**2.08**	**-**	**-**	**-**	
Total capacity of air-turbines (MW)	-	-	7.4	-	-	-	
Annualized cost of air-turbines (MM €)	**-**	**-**	**0.52**	-	-	-	
Total capacity of hydrogen tanks (MWh)	-	-	-	125.5	-	-	
Annualized cost of hydrogen tanks (MM €)	**-**	**-**	**-**	**0.05**	**-**	**-**	
Total capacity of electrolyzers (MW)	-	-	-	5.1	-	-	
Annualized cost of electrolyzers (MM €)	**-**	**-**	**-**	**0.4**	**-**	**-**	
Total capacity of fuel cells (MW)	-	-	-	0.9	-	-	
Annualized cost of fuel cells (MM €)	**-**	**-**	**-**	**0.14**	**-**	**-**	
Total annual network cost (MM €)	**127.45**	**119.54**	**118.66**	**115.4**	**97.3**	**103.25**	**118.55**
Cost per MWh (€/MWh)***	**158**	**148.2**	**147.1**	**143.1**	**120.6**	**128**	**147**

* *The costs of access roads, grid connection and land purchase have not been included,* ** *Thermal power costs different than those in Table IV, will lead to different results,* ***The annual load in Rhode is 806.65 GWh,

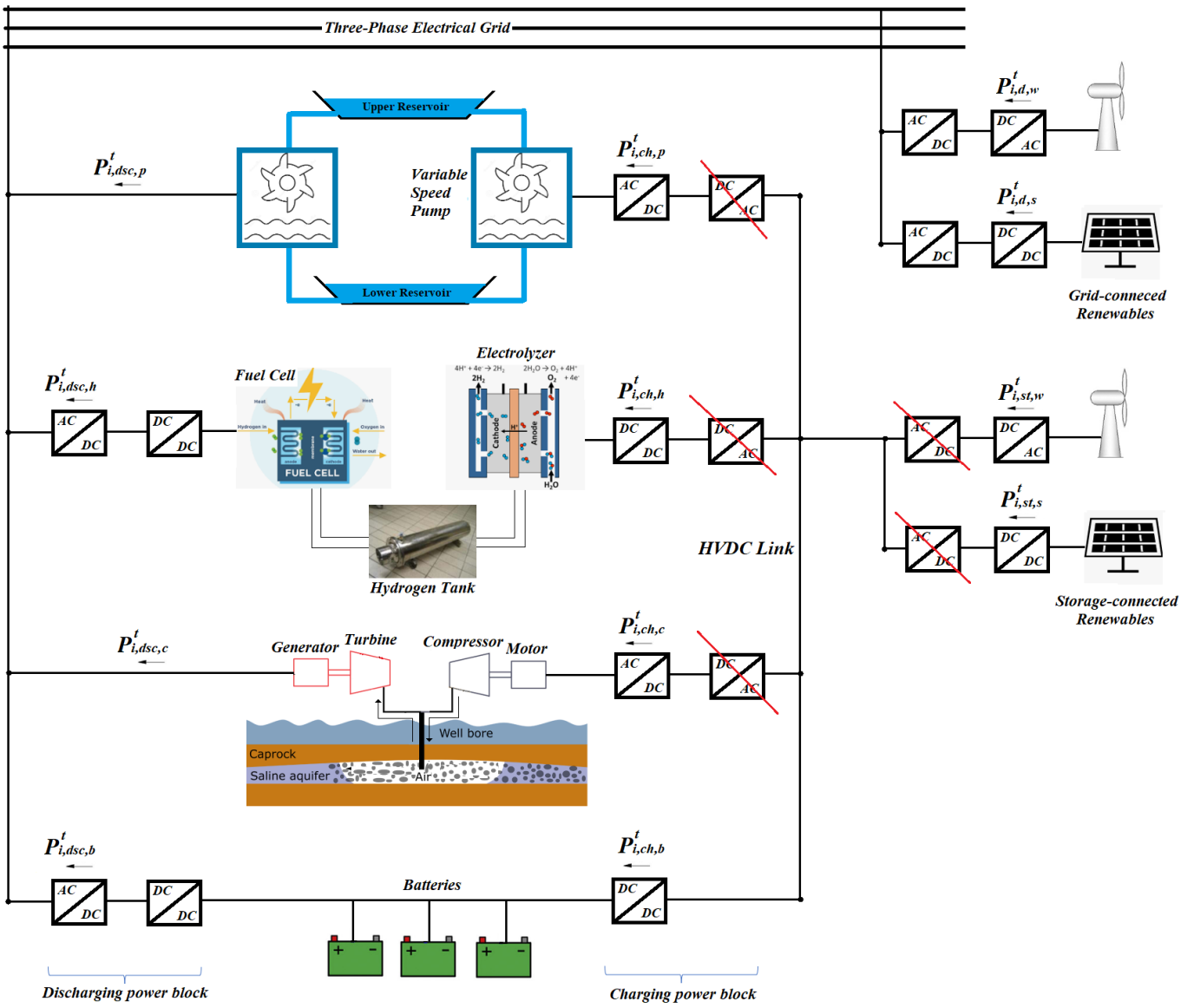

Fig. 1. Proposed HPP configuration consisting of storage- and grid-connected renewables, a double-penstock PHS with variable speed pump, an HSS, a CAES and batteries. Storage-connected renewables are connected to the storage through a common HVDC link, enabling the elimination of one conversion DC/AC stage for PHS, HSS, CAES and storage-connected renewables, improving the overall efficiency of HPP and reducing its installation cost.